Design of Moving Bed Heat Exchangers

Greg Mehos, Ph.D., P.E.
Mark Mehos

Introduction

Concentrated solar power (CSP) systems use heliostats to focus sunlight onto a receiver located at the top of a tall tower. The concentrated sunlight heats a fluid or particles that can be used to provide heat to a conventional turbine to generate power. Moving bed heat exchangers, which consist of vertical heat-transfer plates above a hopper, are used to recover heat from high-temperature particles, allowing greater efficiency, improved thermal storage, and lower costs compared to molten salts [1]. Figure 1 is a schematic of a moving bed heat exchanger.

While there are several publications that describe the transfer of heat from particles to sCO_2 (*e.g*, [2, 3]), design criteria for reliable particle flow are far less documented. This paper details key considerations for designing bulk solids moving bed heat exchangers.

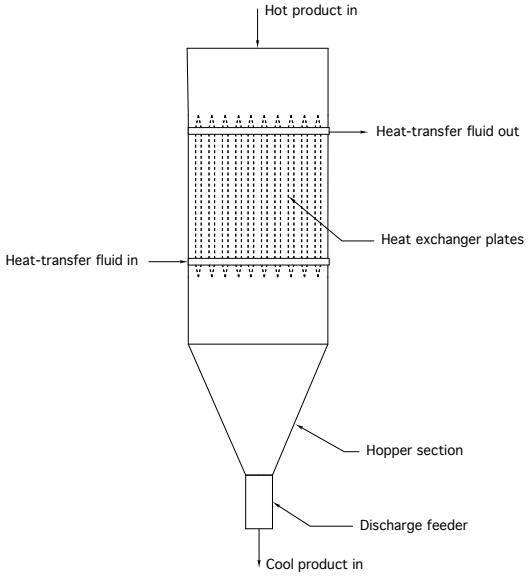

Figure 1. Moving bed heat exchanger schematic.

Bulk solids thermal and flow properties

The rate of heat transfer in a moving bed of solids depends on its thermal properties, *i.e.,* its thermal conductivity and heat capacity. The solids flow behavior depends on fundamental flow properties that include cohesive strength, internal friction, wall friction, and compressibility.

(Specific) heat capacity is measured by differential scanning calorimetry (DSC) where a sample of powder is heated and its rise in temperature is recorded. The response is compared to that from heating a reference material with a known specific heat. A baseline measurement in which no sample is placed in the calorimeter is taken to remove any system bias from the data.

Laser flash analysis (LFA) is used to measure thermal conductivity. A pulse of energy heats one side of a sample of powder and the rise in temperature of the backside is recorded. The thermal diffusivity α is then calculated from

$$\alpha = 0.1388 \frac{d^2}{t_{1/2}} \tag{1}$$

where d is the thickness of the sample and $t_{1/2}$ is the half time to maximum temperature. The thermal conductivity and thermal diffusivity are related by

$$\alpha = \frac{k}{\rho_b C_p} \tag{2}$$

where k is the thermal conductivity, ρ_b is the bulk density, and C_p is the heat capacity. For bulk solids, the thermal conductivity is denoted k_{eff}, *i.e.,* the effective thermal conductivity, as the thermal conductivity of a powder is substantially lower than that of a pure solid.

Noting that the limiting factor of heat transfer in a moving-bed heat is generally the low thermal conductivity of the bulk material, correlations based on void fractions, thermal conductivities of the pure solid and fluid, and empirical constants should be avoided. The value of the effective thermal conductivity should be adjusted downward for material along the wall due to less packing and a greater void volume [4].

The effective specific heat and effective thermal conductivity of sintered bauxite powder are plotted against temperature in Figures 2 and 3, respectively [5].

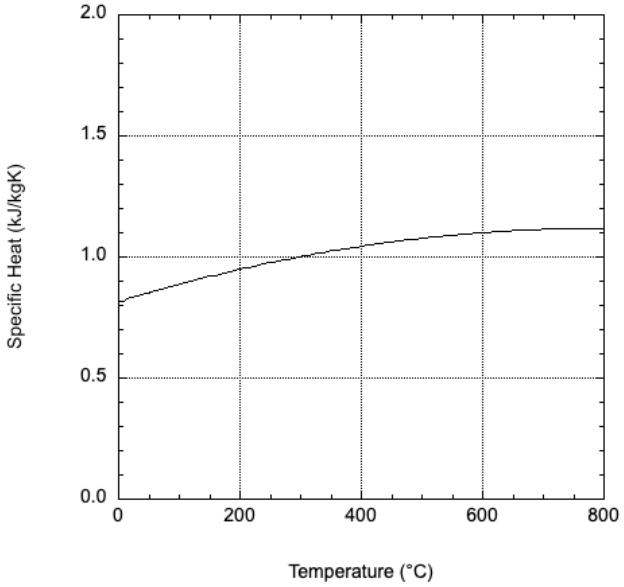

Figure 2. Specific heat capacity of sintered bauxite powder.

Cohesive strength is measured by shear cell testing as described in ASTM D1628 [6], D6682 [7], D6773 [8], or D7891 [9]. A sample of bulk material is placed in a cell and then pre-sheared, *i.e.,* consolidated by exerting a normal stress and then shearing it until the measured shear stress is steady. Next, the shear step is conducted, in which the vertical compacting load is replaced with a smaller load, and the sample is again sheared until it fails. These pre-shear and shear steps are repeated at the same consolidation level for a number of reduced normal stresses, and the yield locus is then determined by plotting the failure shear stress against normal stress (see Figure 4).

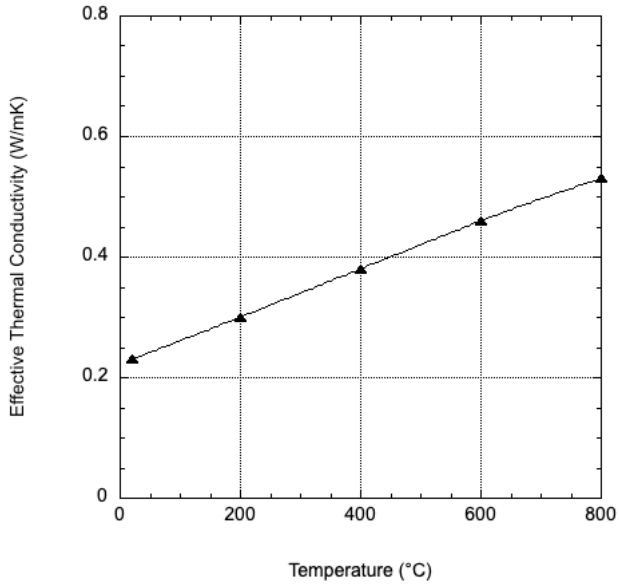

Figure 3. Effective thermal conductivity of sintered bauxite powder.

To determine the major consolidation stress σ_1 and the unconfined yield shear strength f_C from the yield locus, a line is drawn through the shear step data. A Mohr's semicircle is then drawn through the steady-state result tangent to the yield locus line (see Figure 4). Also determined are the effective angle of friction and kinematic angle of internal friction (δ and ϕ, respectively). The effective angle of friction is found by constructing a line through the origin and tangent to the larger Mohr's semicircle. The kinematic angle of internal friction is the angle formed between a line that is horizontal and one drawn tangent to the smaller Mohr's circle at its intersection with the yield locus.

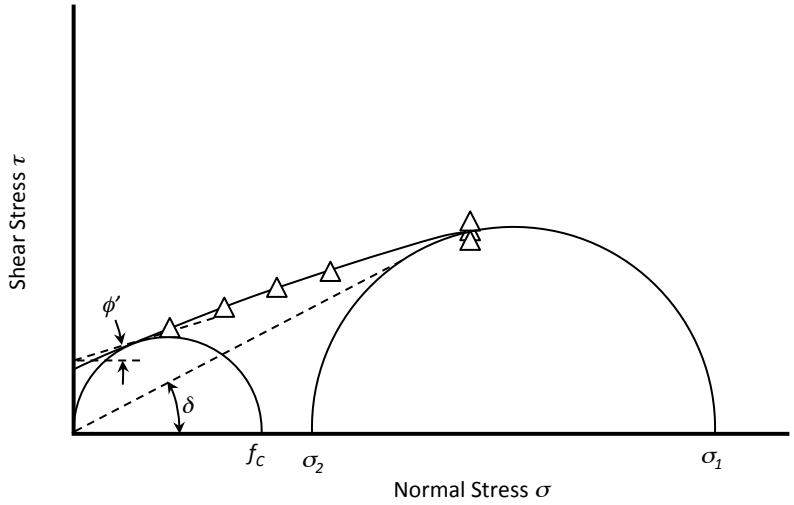

Figure 4. Yield locus.

Plotting values of f_C against the major consolidation stress σ_1 gives the flow function of the bulk solid. The flow function describes the relationship between a bulk material's unconfined yield strength and its state of consolidation.

Bulk density of a material as a function of compressive stress (*i.e.*, pressure) in measured following a procedure given in ASTM D6683 [10]. A sample is placed in a cylinder of known volume and its mass is recorded. A lid with a known weight is placed on the specimen and the displacement is noted, allowing an updated volume to be calculated. The bulk density is equal to the mass of sample divided by its volume. Increasing loads are placed on the lid, and the displacement is recorded for each load. From the data, the bulk density as a function of consolidation pressure is determined. This relationship is frequently called the material's compressibility.

To measure the friction between a bulk solid and a wall material, the method described in ASTM D6128 [6] is usually followed. The test is conducted using a direct translation shear tester. A sample of bulk solid is placed inside a retaining ring on a flat coupon of wall material and a normal load is then applied. The ring and bulk solid in the ring are forced to slide along the stationary wall material, and the resulting steady shear force is measured as a function of the applied normal load. The normal load is then reduced, and the test is continued until a new steady shear load is measured. The test is repeated for various normal loads.

After a few steady shear load values have been recorded, the wall yield locus is constructed by plotting shear stress against normal stress. The angle of wall friction ϕ' is the angle that is formed when a line is drawn from the origin to a point on the wall yield locus (see Figure 5).

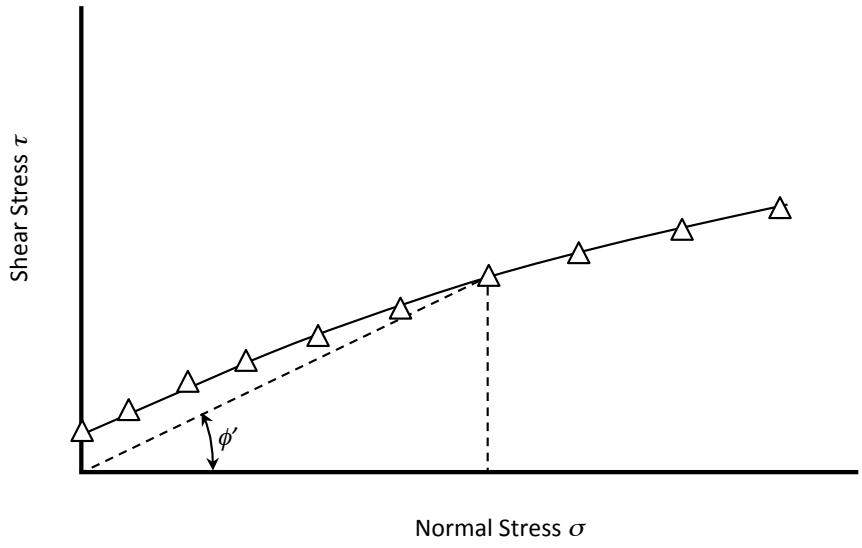

Figure 5. Wall yield locus.

The unconfined yield strength, effective angle of friction, kinematic angle of friction, bulk density, and wall friction on 304 #2B stainless steel of a sample of sintered bauxite are given in Figures 6 through 9.

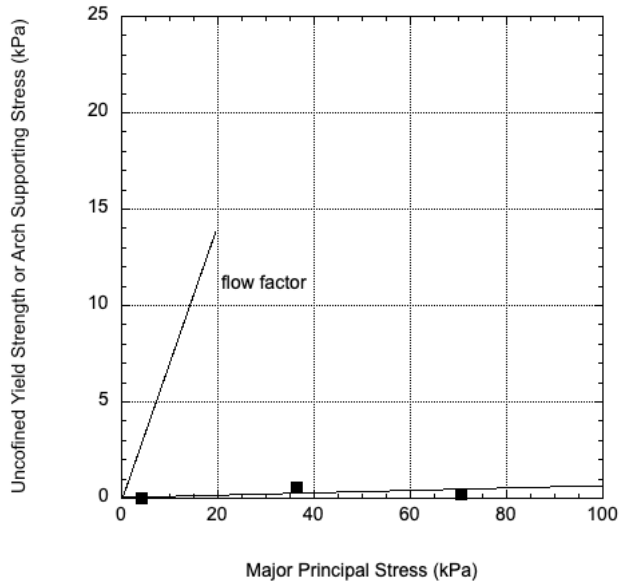

Figure 6. Cohesive strength of sintered bauxite powder.

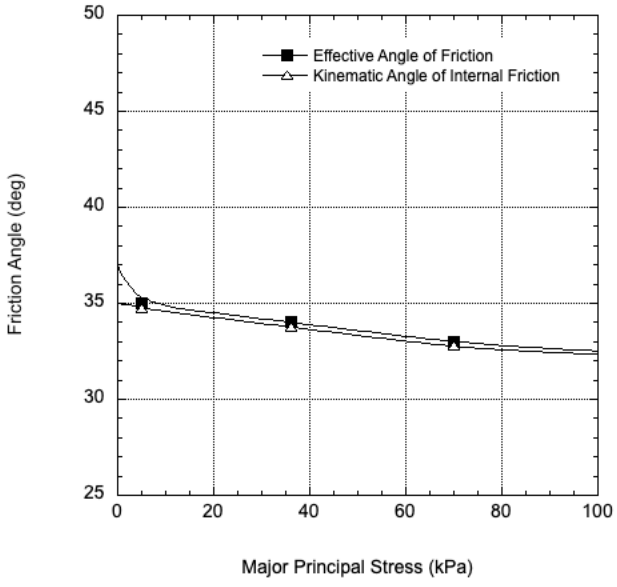

Figure 7. Internal friction of sintered bauxite powder.

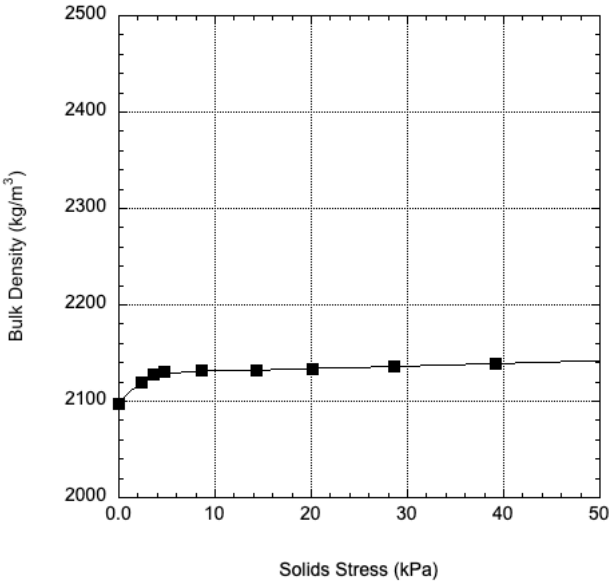

Figure 8. Bulk density of sintered bauxite powder.

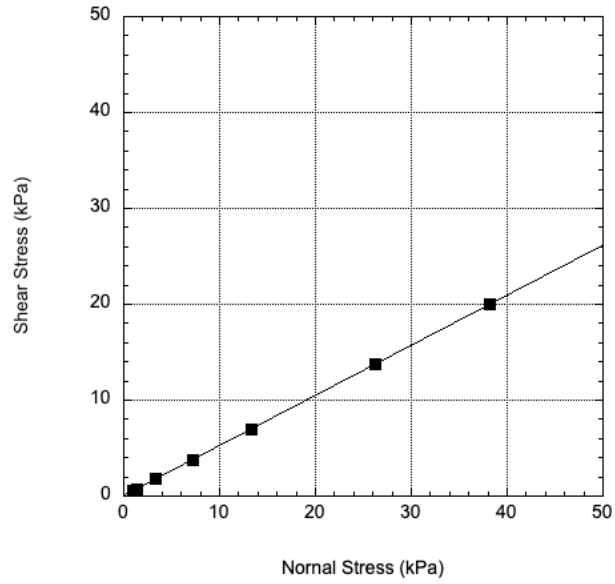

Figure 9. Wall friction of sintered bauxite powder on 304 #2B stainless steel.

Moving bed heat exchanger design criteria

Not only must the moving bed heat exchanger provide the required duty, it must be designed for stable, uniform flow. The hopper section must be designed for mass flow, a pattern in which all material is in motion including along the walls when it is discharged. Otherwise, the pattern will be funnel flow, where particles will only flow in a channel above the outlet.

The recommended mass flow hopper angle θ' depends on the hopper geometry, effective angle of friction δ, and wall friction angle ϕ' and can be calculated using the following formulas for axisymmetric and planar flow, respectively. [11]:

$$\theta' = 87° - \frac{1}{2}\left[\cos^{-1}\left(\frac{1-\sin\delta}{2\sin\delta}\right) - \phi' + \sin^{-1}\left(\frac{\sin\phi'}{\sin\delta}\right)\right] \tag{3}$$

$$\theta' = \frac{\exp[3.75(1.01)^{(\delta-30°)/10°} - \phi'}{0.725(\tan\delta)^{1/5}} \tag{4}$$

Equation 3 includes a 3° safety factor. The recommended planar mass flow hopper angle calculated using Equation 4 can be up to 10° less steep and still allow mass flow.

To prevent bridging, the stress on the abutment of an arch must be greater than its unconfined yield strength. Once a material's flow function has been determined, the minimum outlet width or diameter that will prevent cohesive arching can be calculated, using the hopper's flow factor. Jenike defined the flow factor as the ratio of the major principal stress σ_1 to the arch stress $\bar{\sigma}$, *i.e.*, the external stress applied to the powder at the hopper outlet. From Jenike [12]

$$ff = \frac{\sigma_1}{\bar{\sigma}} \tag{5}$$

Typical values of the flow factor range between 1.1 and 1.7. Johanson [13] provides a convenient chart that displays the flow factor as a function of the effective angle of friction (see Figure 10).

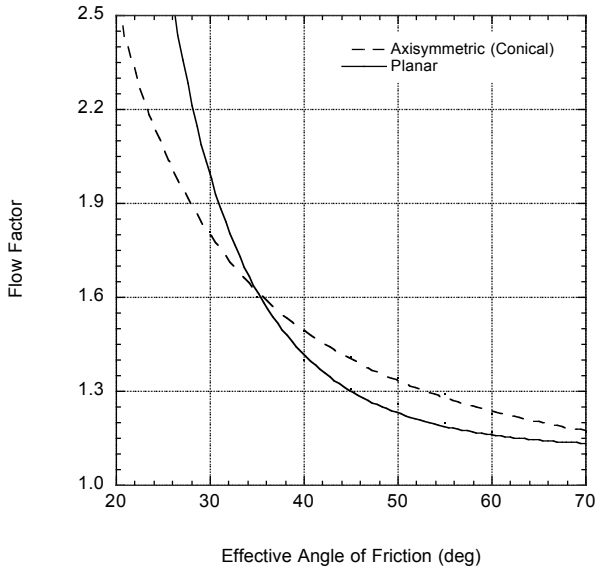

Figure 10. Flow factor vs. effective angle of friction [12].

Superimposing the bulk material's flow function and flow factor on the same graph allows the cohesive strength of the material at the hopper outlet and arch stress to be compared. If the flow function lies below the flow function, then the stress on the arch is always greater than the material's strength, and arching will not occur. If the flow function lies above the flow factor and the curves do not intersect, gravity flow is not possible. If the flow function and flow factor

intersect as shown in Figure 11, then the minimum outlet dimension that prevents arching can be calculated from:

$$B_{\min} = \frac{H(\theta')\sigma_{criti}}{\rho_b g} \tag{6}$$

where B_{min} is the critical outlet diameter of a conical hopper or width of a planar hopper, $H(\theta')$ is a shape factor given in Jenike [12] approximately equal to 2 for hoppers with round outlets and approximately 1 for planar hoppers with slotted outlets, σ_{crit} is the critical stress (see Figure 11), and g is acceleration due to gravity.

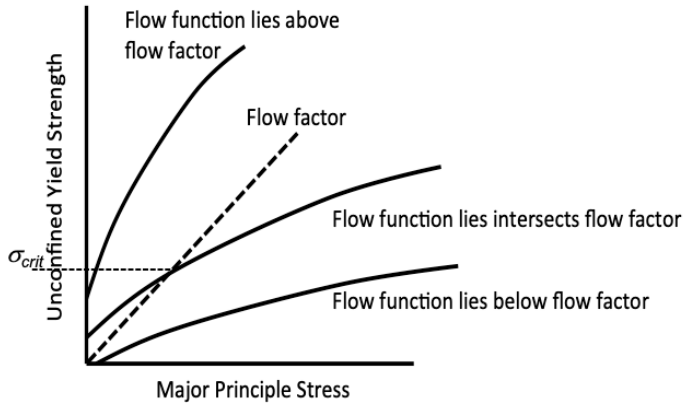

Figure 11. Plot of flow function and flow factor.

For non-cohesive materials, very small outlets can be used and are typically set equal to 3-4 times the maximum particle dimension. This is also often the criterion used for specifying plate spacing. For less flow-freeing materials, a flow factor of 1.7 can be used to calculate the critical stress σ_{crit} that is used in Equation 6 to calculate the width.

For the bauxite tested, the valleys of a pyramidal hopper or the side walls of a wedge-shaped hopper must be sloped 12° or 24° from vertical, respectively, to ensure mass flow. In general, planar hoppers are preferable as funnel flow is less likely and because moving bed heat exchangers have square or rectangular cross sections.

When particles flow into the hopper section, a passive state of stress develops in which the maximum stresses align horizontally rather than vertically (see Figure 12). If the bottom of the plates is located too close to the inlet to the hopper, flow instabilities can develop. This critical distance depends on the effective angle of friction, hopper angle and wall friction angle, and it can be calculated following an analysis given by Jenike [12].

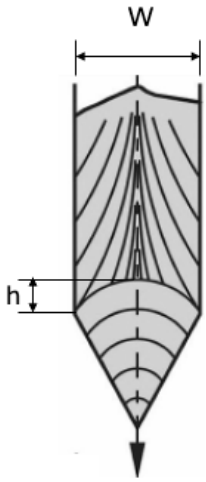

Figure 12. Passive state of stress extending from hopper section.

$$\frac{d\psi}{d\theta} = -1 - [ms\sin\delta(1+\sin\delta)(\cot\theta\sin 2\psi + \cos 2\psi - 1) + \cos\theta - \sin\delta\cos(\theta+2\psi) + s\cos^2\delta] / [2s\sin\delta(\cos 2\psi - \sin\delta)] \tag{7}$$

$$\frac{ds}{d\theta} = \frac{s\sin 2\psi + \sin(\theta+2\psi) + ms\sin\delta[\cot\theta(1+\cos 2\psi) - \sin 2\psi]}{\cos 2\psi - \sin\delta} \tag{8}$$

where s is Jenike's radial stress function, ψ is the angle between the radial coordinate ray and the principal stress, and m is equal to 1 or 0 for axisymmetric and planar flow, respectively. For Boundary conditions are:

$$\psi(\theta') = \frac{1}{2}\left[\phi' + \sin^{-1}\left(\frac{\sin\phi'}{\sin\delta}\right)\right] + 90° \tag{9}$$

$$\psi(90°) = 90° \tag{10}$$

From these equations can be calculated the magnitude and direction of the principal solids stresses. Results for sintered bauxite are given in Figure 13. The recommended minimum distance between the bottom of the heat exchanger and the start of the hopper is 0.3 times its width.

To control the discharge rate from the moving bed heat exchanger, a feeder is used. For hoppers with round or square outlets, rotary valves are common. For planar hoppers with slotted outlets, screw feeders are frequently used.

The capacity of the screw must increase in the direction of discharge; otherwise, preferential flow may occur, resulting in stagnant regions in the heat exchanger. This is accomplished by having tapered shaft and increasing pitch sections in the screw. Figure 14 illustrates the design of a mass-flow screw feeder.

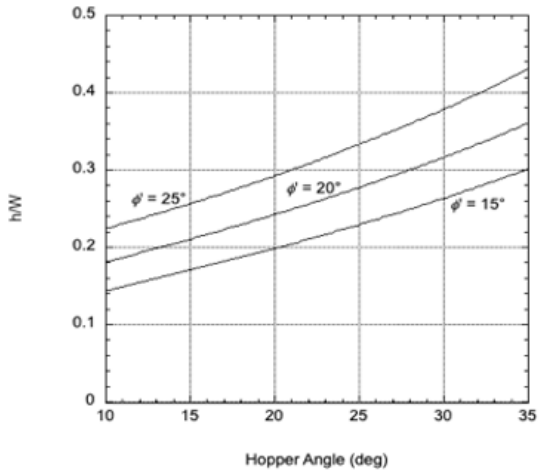

Figure 13. Minimum distance between heat exchanger plate exit and hopper inlet when handling sintered bauxite ($\delta = 35°$).

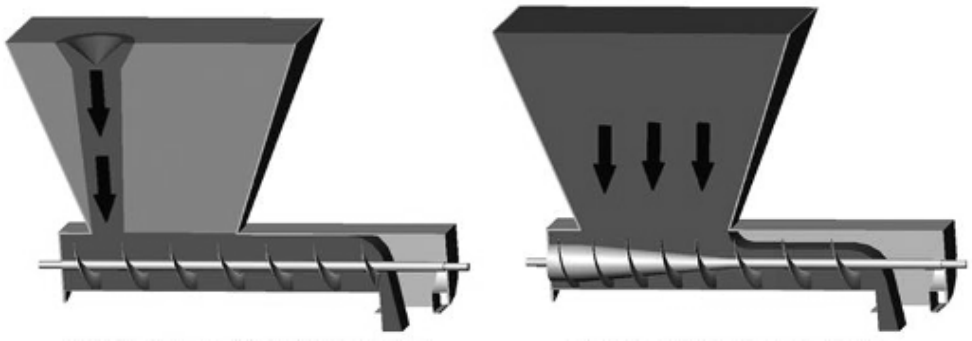

Figure 14. Screw feeders – left: constant pitch screw feeder; right: screw feeder with tapered shaft and increasing pitch sections (mass-flow feeder).

Louvre vibratory feeders are sometimes used. They should be placed at the hopper inlet and material should not be allowed to accumulate in the hopper section,

While slide gates are generally not recommended for modulating discharge rates, they can be used with easy-flowing powders that do not degrade when remaining at rest. A vertical section should be installed between the gate and the hopper outlet. The particle flow in this section will behave like a flat-bottomed silo with a slotted outlet that gives an expanding flow channel. The sliding gate valve should be installed such that they are opened from beneath the side walls and not the end walls to ensure that the flow channel expands to the walls. Otherwise, the opening will not be a slot, and the flow channel will be steep and remain narrow inside the hopper and heat exchanger sections.

The flow channel angle $\theta_{\phi\chi}$ can be estimated from Equation 11 [14]. The flow channel angle for axisymmetric (round or square outlets) and planar (slotted outlets) flow is plotted against effective angle of friction in Figure 15.

$$\theta_{fc} = \left[45° - \frac{1}{2}\cos^{-1}\left(\frac{1-\sin\delta}{2\sin\delta}\right)\right]^{m}\left[65° - \frac{1}{2}\cos^{-1}\left(\frac{1-\sin\delta}{\sin\delta}\right)\right]^{m-1} \tag{11}$$

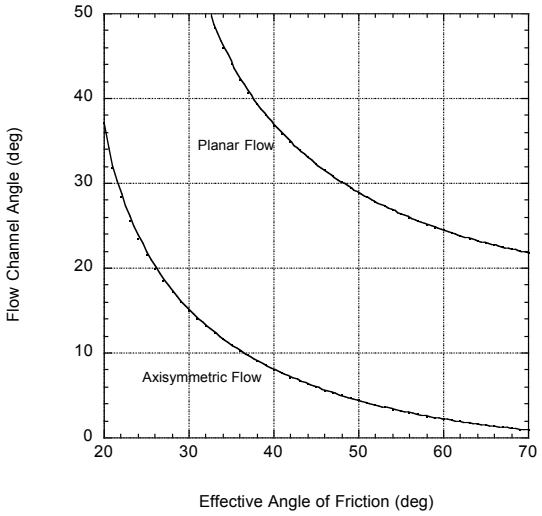

Figure 15. Flow channel angle.

The discharge rate will be proportional to B to the 5/2 power. For coarse particles, it can be predicted using the material's cohesive strength and flow factor by [15]:

$$\dot{m}_s = \rho_{bo} A_o \sqrt{\frac{Bg}{2(m+1)\tan\theta'}\left(1 - \frac{ff}{ff_a}\right)} \tag{12}$$

where ff_a is the material's actual flow factor and is equal to the ratio of the solids stress at the hopper outlet to its unconfined yield strength. Unless the particles are non-cohesive, however, there will be no discharge from the slide gate until the width of the opening B reaches the value of B_{min} calculated from Equation 6.

The moving bed heat exchanger must be sized to accomplish the required duty. Consider the streams of bulk solids and fluid flowing countercurrently inside the plates of a moving-bed heat exchanger shown in Figure 16. The plates are separated by a distance b, and the height of a plate L.

Fourier's law is used to describe heat transfer in the solids stream:

$$\rho_b u_s C_{ps} \frac{\partial T_s}{\partial z} = -k_{eff} \frac{\partial^2 T_s}{\partial x^2} \tag{13}$$

where ρ_b is the bulk density, u_s is the solids velocity, C_{ps} is the solids specific heat, T_s is the solids temperature, k_{eff} is the effective thermal conductivity, and x and z are the horizontal and vertical coordinates, respectively. Boundary conditions are:

$$-k'_{eff} \frac{\partial T_s(\pm\frac{b}{2}, z)}{\partial x} = U_o[(T_s(\pm\tfrac{b}{2}, z) - T_f] \tag{14}$$

$$T_s(x,0) = T_{s0}(x) \tag{15}$$

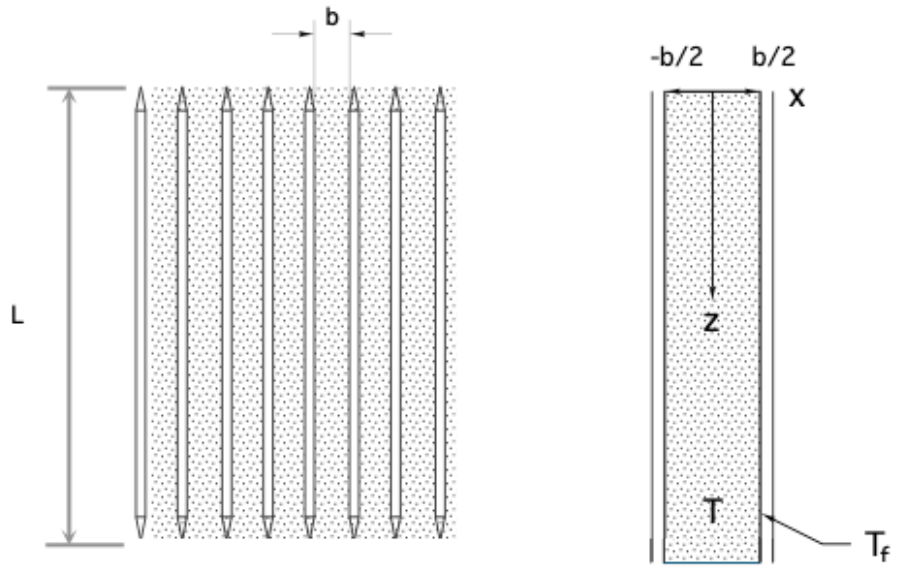

Figure 16. Moving bed heat exchanger schematic.

where k'_{eff} is the effective thermal conductivity of the bulk solid at the wall and U_o is the overall heat transfer coefficient, which includes resistances due to convection in the fluid phase, radiation, and conduction through particles near the wall. Resistance through the heat exchanger wall itself can be considered negligible.

Equation 16 is an overall energy balance that allows calculation of the fluid temperature T_f:

$$d(u_s \rho_b C_{ps} \bar{T}_s) = d(u_f \rho_f C_{pf} T_f) \tag{16}$$

where ρ_f is the density of the fluid and C_{ps} is its heat capacity.

Consider the moving bed heat exchanger described by Fang et al. [2], where the plate spacing was 10 mm, its length equal to 1 m, and the particle and fluid (sCO_2) velocities equaled 0.001 m/s and 0.2 m/s, respectively. In the analysis, the following correlations were used together with the fluid properties given in [2]:

Fluid side:

$$\mathrm{Nu} = 0.00292\ \mathrm{Re}^{0.8}\mathrm{Pr}^{1/3} \tag{17}$$

$$\mathrm{Nu} = \frac{hL}{k} \tag{18}$$

$$\mathrm{Pr} = \frac{C_p \eta}{k} \tag{19}$$

$$\mathrm{Re} = \frac{\rho_f u_f L}{\eta} \tag{20}$$

where Nu is the Nusselt number, Pr is the Prandtl number, Re is the Reynolds number, h is the local heat-transfer coefficient, L is the length, k is the thermal conductivity of the fluid, η is the fluid viscosity, ρ_f is the density of the fluid, and u_f is the fluid velocity.

Radiation:

$$h_r = 4\varepsilon\sigma T^3 \tag{21}$$

where ε is the emissivity, σ is the Stefan-Boltzmann constant (5.67×10^{-8} W/m^{2}K^4), and T is the typically chosen as the average absolute temperature.

Particles near wall:

$$h_{pbl} = \frac{k'_{eff}}{d_p} \tag{22}$$

where h_{pbl} is the local heat transfer coefficient at the wall boundary (particle side), k'_{eff} is the effective thermal conductivity of the bulk solid near the wall, and d_p is the particle diameter.

Figure 17 compares predicted temperatures in the moving bed heat exchanger streams. Calculated solids temperature profiles within the plates are shown in Figure 18.

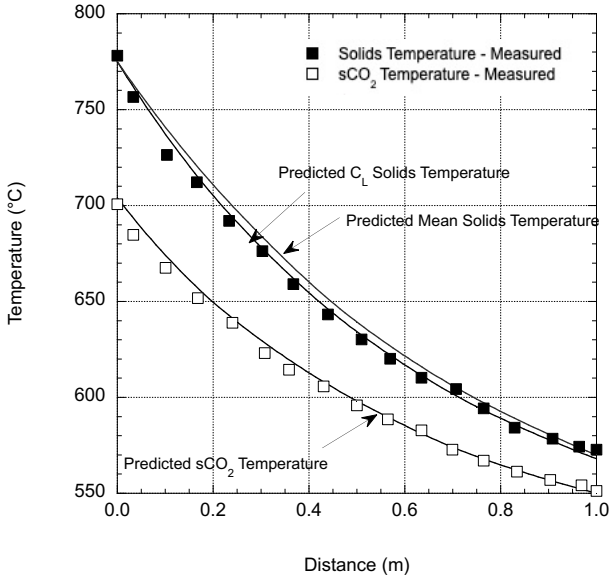

Figure 17. Comparison of predicted and observed temperature profiles.

Because a 20-mm plate spacing can be risky because of possible blockage between the heat exchanger, increasing the spacing may be prudent. However, the rate of heat transfer will be reduced and greater heat transfer area will be required. This can be accomplished by either using longer plates or installing banks of plates that are offset as shown in Figure 19. Calculations suggest that having two banks of plates spaced 20 mm apart and each 0.55 m long will allow the same fluid and particle inlet and outlet temperatures. Temperature profiles are shown in Figure 20.

Final remarks

A moving-bed heat exchangers is basically a silo or hopper that includes heat-transfer plates in its vertical-walled section. Heat transfer through the moving packed bed of solids can be modelled using Fourier's Law with appropriate boundary conditions. The hopper section of the process vessel should have walls steep enough for mass flow to prevent stagnant regions within the heat exchanger plates. In addition, there must be sufficient distance between the bottom of the plates and the start of the hopper section to prevent particle flow instabilities.

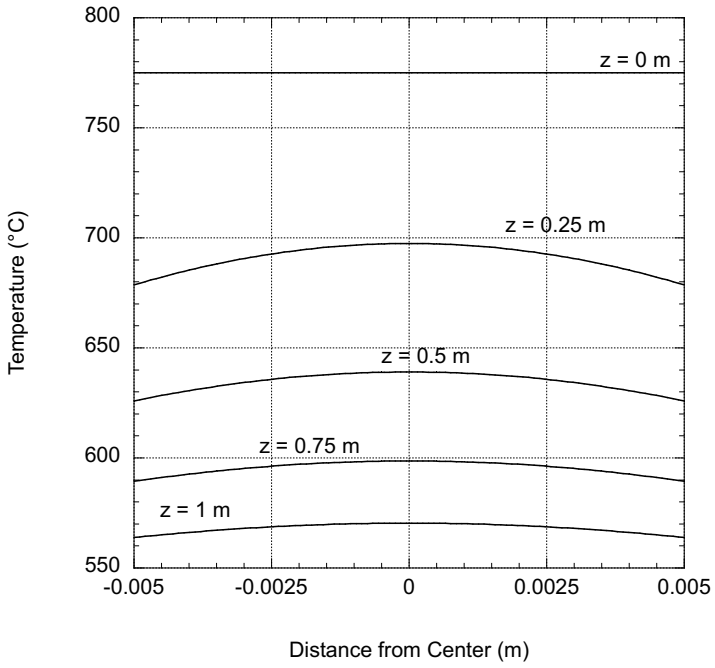

Figure 18. Measured and predicted temperatures.

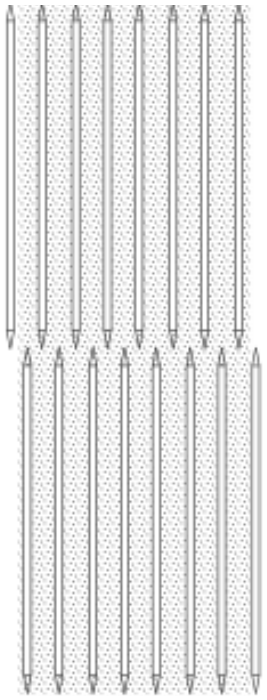

Figure 19. Staggered banks.

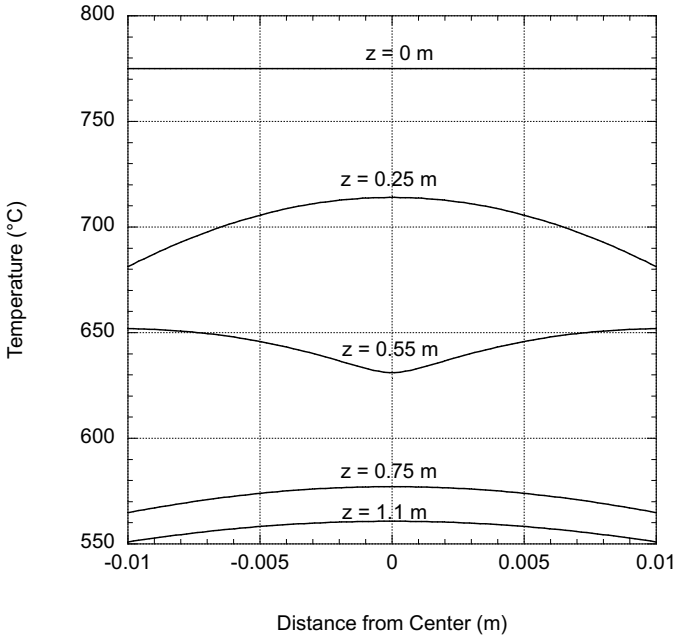

Figure 20. Solids temperature profiles – two banks.

References

[1] Mehos, M. et al., "Concentrating Solar Power Gen3 Demonstration Roadmap", NREL/TP-5500-67464. National Renewable Energy Lab., Golden, CO USA (2017).

[2] Fang, W., S. Chen, J. Xu, and K. Zeng., "Predicting Heat Transfer Coefficient of a Shell-and-Plate, Moving Packed-Bed Particle-to-sCO2 Heat Exchanger for Concentrating Solar Power", Energy 217 (2021).

[3] Albrecht, K. and C, Ho, "Design and Operating Considerations for a Shell-and-Plate, Moving Packed Bed Particle-to-sCO2 Heat Exchanger", Solar Energy, 278 (2019).

[4] Watkins M., Y. Chilamkurti, and R. Gould "Analytic Modelling of Heat Transfer to Vertical Dense Granular Flows", *J. Heat Transfer*, 142, 2 (Feb 2020).

[5] Baumann, T. and S. Zunft, Properties of Granular Materials as Heat Transfer and Storage Medium in CSP Application", Solar Energy Materials & Solar Cells, 143, 38 (2015).

[6] ASTM D6128, Standard Test Method for Shear Testing of Bulk Solids Using the Jenike Shear Cell, 1 International, 2023.

[7] ASTM D6682, Standard Test Method for Measuring the Shear Stresses of Powders Using the Peschl Rotational Split Level Shear Tester, ASTM International, 2017.

[8] ASTM D6773, Standard Test Method for Bulk Solids Using Schulze Ring Shear Tester, ASTM International, 2023.

[9] ASTM D7891, Standard Test Method for Shear Testing of Powders Using the Freeman Technology FT4 Powder Rheometer Shear Cell, ASTM International, 2024.

[10] ASTM D6683, Standard Test Method for Measuring Bulk Density Values of Powders and Other Bulk Solids as Function of Compressive Stress, ASTM International, 2019.

[11] Arnold, P., A. Roberts, and A. McLean, Bulk Solids: Storage, Flow, and Handling, TUNRA, Newcastle, Australia, 1978.

[12] Jenike, A.W., Gravity flow of Bulk Solids, Bulletin 108, University of Utah, 1961.

[13] Kulwiec, R., Materials Handling Handbook, John Wiley and Sons, Hoboken, NJ, 1985.

[14] Mehos, G., Storage and Flow of Bulk Solids, Greg Mehos and Associates, 2025.

[15] Mehos, G., "Using Solids Flow Properties to Design Mass- and Funnel-Flow Hoppers", Powder Bulk Engr., 34, 2 (February 2020).